

# Full quantum theory for magnon transport in two-sublattice magnetic insulators and magnon junctions

Tianyi Zhang<sup>1</sup> and Xiufeng Han<sup>1,2,3,\*</sup>

<sup>1</sup>Beijing National Laboratory for Condensed Matter Physics, Institute of Physics, Chinese Academy of Sciences, Beijing 100190, China

<sup>2</sup>Center of Materials Science and Optoelectronics Engineering, University of Chinese Academy of Sciences, Beijing 100049, China

<sup>3</sup>Songshan Lake Materials Laboratory, Dongguan, Guangdong 523808, China



(Received 4 April 2023; accepted 15 September 2023; published 26 September 2023)

Magnons, as elementary excitations in magnetic systems, can carry and transfer angular momentum. Due to the absence of Joule heat during magnon transport, research on magnon transport has gained considerable interest over the past decade. Recently, a full quantum theory has been employed to investigate magnon transport in ferromagnetic insulators (FMIs). However, the most commonly used magnetic insulating material in experiments, yttrium iron garnet (YIG), is a ferrimagnetic insulator (FIMI). Therefore a full quantum theory for magnon transport in FIMIs needs to be established. Here, we propose a Green's function formalism to compute the bulk and interface magnon currents in both FIMIs and antiferromagnetic insulators (AFMIs). We investigate the spatial distribution and temperature dependence of magnon currents in FIMIs and AFMIs generated by a temperature or spin chemical potential step. In AFMIs, magnon currents generated by a temperature step in the two sublattices cancel each other out. Subsequently, we numerically simulate the magnon junction effect using the Green's function formalism, and the results show a near 100% magnon junction ratio. This study demonstrates the potential of using a full quantum theory to investigate magnon transport in specific magnonic devices.

DOI: [10.1103/PhysRevB.108.104421](https://doi.org/10.1103/PhysRevB.108.104421)

## I. INTRODUCTION

Magnons, which are the elementary excitations in magnetic systems [1–3], have potential to serve as information carriers due to their ability to carry and transfer angular momentum. Compared to electrons, using magnons for information transport offers three main advantages. Firstly, magnons can transport in magnetic insulators, which avoids the generation of Joule heat [4]. Secondly, magnons are ideal carriers for transporting GHz or THz information [5–9]. Thirdly, there are multiple methods to inject and detect magnon currents. The injection methods include microwave antennas [10–12], the spin Seebeck effect (SSE) [4,13–16], and the spin Hall effect (SHE) [17]. The detection methods include Brillouin light scattering [18] and the inverse spin hall effect (ISHE) [19,20]. Recently, there has been increased research on spin transport involving magnons, such as magnon-mediate drag effect [21,22], magnon valve effect [23–26], and magnon junction effect [27]. Similar to the metal-oxide-semiconductor field-effect transistor (MOSFET) in microelectronic devices, a magnon junction, consisting of a ferromagnetic insulator (FMI1)/antiferromagnetic insulator (AFMI)/ferromagnetic insulator (FMI2), is an elementary device that controls the opening and closing of magnon transport channels. To be more specific, we can control the magnitude of the output magnon current by manipulating the magnetization state of the two FMI layers. The output magnon current

is larger for the parallel state and smaller for the antiparallel state.

For a deeper understanding of the experimental phenomenon, numerous theories have been proposed to investigate magnon transport. One widely used classical equation for calculating magnon accumulation and transport [28,29] is the LLG (Landau-Lifshitz-Gilbert) equation, initially introduced by Landau and Lifshitz, and later modified by Gilbert [30]. Another approach is the magnon Schrödinger equation, which is employed to study the wave properties and coherent transport of magnons [31–38]. The magnon Boltzmann function [39–42] is used to describe magnon transport from a particle perspective. Recently, Duine *et al.* proposed a Green's function formalism to elucidate magnon transport in FMIs, with and without anisotropy terms [43,44]. The advantage of this approach lies in proposing a complete quantum theory for calculating magnon transport, facilitating the consideration of disorder and the coupling of magnons with other particles or quasi-particles. However, in experimental studies, yttrium iron garnet (YIG), a ferrimagnetic insulator (FIMI), is one of the most commonly used magnetic materials, thereby necessitating the development of a Green's function formalism specifically tailored for FIMIs.

In this paper, we present an analytical derivation of the Green's function formalism for magnon transport in FIMIs or AFMIs. Our analysis reveals the existence of two distinct effective magnon currents in FIMIs or AFMIs, which do not interact with each other. Furthermore, we investigate the spatial distribution of magnon currents induced by temperature or spin chemical potential steps in FIMIs or AFMIs.

\*xfhan@iphy.ac.cn

Additionally, we calculate the temperature dependence of magnon current, which is consistent with previous research [22]. Then, we study the magnon transport in a magnon junction, simulating the magnon junction effect and the result shows near 100% magnon junction ratio. Our work demonstrates the potential of utilizing the Green's function formalism to investigate magnon transport in specific magnonic devices.

## II. MODEL AND METHOD

The Hamiltonian for the FIMI or AFMI systems, considering Zeeman energy, nearest and next-nearest neighbor Heisenberg exchange interactions, is expressed as follows:

$$\begin{aligned} \hat{H} = & -J_{AB} \sum_{\langle i,m \rangle} \hat{S}_i \cdot \hat{S}_m - J_A \sum_{\langle\langle i,j \rangle\rangle} \hat{S}_i \cdot \hat{S}_j \\ & - J_B \sum_{\langle\langle m,n \rangle\rangle} \hat{S}_m \cdot \hat{S}_n - h_{\text{ext}} \left( \sum_i \mu_A \hat{S}_i^z + \sum_m \mu_B \hat{S}_m^z \right), \end{aligned} \quad (1)$$

where the subscribe  $\langle \dots \rangle$  denotes summing over nearest sites,  $\langle\langle \dots \rangle\rangle$  denotes summing over next-nearest sites.  $J_{AB} < 0$  and  $J_{A(B)} > 0$  represent the nearest and next-nearest Heisenberg exchange interactions energy, respectively.  $S_{i(m)}$  is the spin in A(B) sublattice,  $\mu_{A(B)}$  is the magnetic moment in A(B) sublattice.  $h_{\text{ext}}$  is applied magnetic field along the z direction. Using Holstein-Primakoff (HP) transformation [2], Fourier transformation and Bogoliubov transformation (Details are shown in the Appendix A), we can get

$$\begin{aligned} \hat{H} = & \sum_k \left[ \left[ \frac{A_k - B_k}{2} + \frac{\sqrt{(A_k + B_k)^2 - 4C_k^2}}{2} \right] \hat{\alpha}_k^\dagger \hat{\alpha}_k \right. \\ & \left. + \left[ \frac{-A_k + B_k}{2} + \frac{\sqrt{(A_k + B_k)^2 - 4C_k^2}}{2} \right] \hat{\beta}_k^\dagger \hat{\beta}_k \right] + \text{const} \\ \equiv & \sum_k (w_k^\alpha \hat{\alpha}_k^\dagger \hat{\alpha}_k + w_k^\beta \hat{\beta}_k^\dagger \hat{\beta}_k) + \text{const}, \end{aligned} \quad (2)$$

where  $\hat{\alpha}_k$  ( $\hat{\beta}_k$ ),  $\hat{\alpha}_k^\dagger$  ( $\hat{\beta}_k^\dagger$ ) are magnon annihilation and creation operators in A(B) sublattice, respectively. And  $\alpha$  ( $\beta$ ) mode magnons have the spin polarization direction parallel to the direction of magnetic moment in sublattice A(B).  $A_k \equiv -2J_A S_A \gamma_{k,nn} - J_{AB} S_B N_n + 2J_A S_A N_{nn} + h_{\text{ext}} \mu_A$ ,  $B_k \equiv -2J_B S_B \gamma_{k,nn} - J_{AB} S_A N_n + 2J_B S_B N_{nn} - h_{\text{ext}} \mu_B$ ,  $C_k \equiv -J_{AB} \sqrt{S_A S_B} \gamma_{k,n}$ ,  $N_n$ ,  $N_{nn}$  are the numbers of nearest and the next-nearest sites, respectively. In the case of one-dimensional atomic chain model,  $N_n = N_{nn} = 2$ ,  $\gamma_{k,n} = 2 \cos(ka)$ ,  $\gamma_{k,nn} = 2 \cos(2ka)$ , where  $a$  is the distance between nearest sites. Thus, in both FIMI or AFMI systems, the magnon currents can be separated into two uncoupled currents with opposite polarities. Specifically, in AFMI,  $J_A = J_B$ ,  $S_A = S_B$ ,  $\mu_A = \mu_B$ , but in FIMI, the above equation does not hold.

Equation (2) shows that in both FIMI and AFMI systems, there exist two distinct types of independent magnons. We can use Fourier transformation to Eq. (2) to transform Hamiltonian of FIMI or AFMI to the summation in coordinate space, and get

$$w_k^{\alpha(\beta)} = \sum_{n=0}^{\infty} 2A_n(B_n) \cos(nka), \quad (3)$$

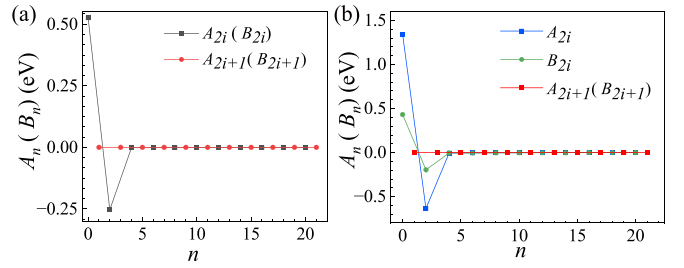


FIG. 1. The variation of the Fourier expansion coefficient with expansion order  $n$  for (a) AFMI and (b) FIMI. The parameters are shown as follows, (a)  $J_{AB} = -0.002$  eV,  $J_A = J_B = 0.02$  eV,  $S_A = S_B = 1$ ; and (b)  $J_{AB} = -0.005$  eV,  $J_A = 0.05$  eV,  $J_B = 0.01$  eV,  $S_A = 1$ ,  $S_B = 1.5$ .

Hamiltonian of FIMI or AFMI to the summation in coordinate space, and get

$$\hat{H} = \sum_{n=0}^{\infty} \sum_{i,j} \delta_{i-j \pm n} (A_n \hat{\alpha}_i^\dagger \hat{\alpha}_j + B_n \hat{\beta}_i^\dagger \hat{\beta}_j). \quad (4)$$

From Eqs. (2)–(4), we can see that for a one-dimensional atomic chain model  $A_{2i+1} = B_{2i+1} = 0$  ( $i = 0, 1, 2, \dots$ ), details of calculation are shown in Appendix B. Then we investigate the variation of the Fourier expansion coefficient with expansion order, as shown in Fig. 1, where for AFMI we use the following parameters [45,46]:  $J_{AB} = -0.002$  eV,  $J_A = J_B = 0.02$  eV,  $S_A = S_B = 1$ , and for FIMI we use the following parameters [29]:  $J_{AB} = -0.005$  eV,  $J_A = 0.05$  eV,  $J_B = 0.01$  eV,  $S_A = 1$ , and  $S_B = 1.5$ . We can see that for both AFMI and FIMI the odd parts of the expansion coefficients are consistently 0, while the even parts approach 0 when  $n \geq 4$ , indicating that only two terms  $A_0(B_0)$  and  $A_2(B_2)$  need to be retained.

Next, we investigate the magnon transport in FIMI or AFMI systems, considering only two terms  $A_0(B_0)$  and  $A_2(B_2)$ . Figure 2 presents a schematic diagram depicting the magnon current transport through FIMI or AFMI. The FIMI



FIG. 2. Schematic diagram that illustrates the transport of magnon current through FIMI or AFMI driven by temperature or spin chemical potential step.

or AFMI is connected to two normal metals (NMs) with temperatures  $T_R$ ,  $T_L$  and spin chemical potentials  $\mu_L$ ,  $\mu_R$ , respectively. The magnon current arises from the temperature or spin chemical potential difference between two NMs. To compute the bulk magnon current, we first calculate the retarded and advanced Green's functions using the Dyson equation

$$\mathcal{G}^{R(A)}(\varepsilon) = [\varepsilon^{+(-)} - H - \hbar \Sigma^{R(A)}(\varepsilon)]^{-1}, \quad (5)$$

where  $\mathcal{G}^{R(A)}$  is retarded (advanced) Green's function,  $\varepsilon^{+(-)} = \varepsilon + (-)i\eta$ ,  $\eta$  is a infinitesimal positive number,  $H$  is Hamiltonian for the FIMI or AFMI systems, and  $\Sigma^{R(A)}(\varepsilon)$  is retarded(advanced) self-energy, which describes the coupling between FIMI or AFMI and external environment. According to Eq. (4), considering the first two terms of the expansion, the Hamiltonian for the FIMI or AFMI systems is

$$\hat{H} = \sum_{i,j} [(A_0\delta_{i,j} + A_2\delta_{i,j\pm 2})\hat{\alpha}_i^\dagger \hat{\alpha}_j + (B_0\delta_{i,j} + B_2\delta_{i,j\pm 2})\hat{\beta}_i^\dagger \hat{\beta}_j] \quad (6)$$

and the self-energy is composed of three items  $\Sigma^R(\varepsilon) = \Sigma_C^R(\varepsilon) + \Sigma_L^R(\varepsilon) + \Sigma_R^R(\varepsilon)$ , where

$$\begin{aligned} \Sigma_C^R(\varepsilon) &= -i\alpha(\varepsilon - \mu_C)\delta_{i,j}/\hbar, \\ \Sigma_L^R(\varepsilon) &= -i\eta^L(\varepsilon - \mu_L)\delta_{i,j}(\delta_{j,1} + \delta_{j,2})/\hbar, \\ \Sigma_R^R(\varepsilon) &= -i\eta^R(\varepsilon - \mu_R)\delta_{i,j}(\delta_{j,N} + \delta_{j,N-1})/\hbar \end{aligned} \quad (7)$$

are retarded self-energy induced by Gilbert damping in FIMI or AFMI, connection with left NM and right NM, respectively. Where  $\alpha$  is Gilbert damping constant,  $\hbar$  is reduced Planck's constant,  $\eta^{L(R)}$  is parameter that represents the coupling with left and right NMs [44,47],  $\mu_{L(R)}$  is spin chemical potential of left(right) NM,  $\mu_C$  is magnon potential of FIMI or AFMI.

Secondly, we can calculate the magnon density matrix using Langreth rule, take  $\alpha$  mode magnon as an example [44]

$$\rho = \langle \hat{\alpha}^\dagger \hat{\alpha} \rangle = \int_{-\infty}^{\infty} \frac{d\varepsilon}{2\pi} [\mathcal{G}^R(\varepsilon) i\hbar \Sigma^<(\varepsilon) \mathcal{G}^A(\varepsilon)], \quad (8)$$

where the lesser self-energy can be calculated by

$$\begin{aligned} \Sigma^<(\varepsilon) &= \Sigma_C^<(\varepsilon) + \sum_{r \in \{L,R\}} \Sigma_r^<(\varepsilon) \\ &= 2iN_B \left( \frac{\varepsilon - \mu_C}{k_B T_C} \right) \text{Im}(\Sigma_C^R(\varepsilon)) \\ &\quad + \sum_{r \in \{L,R\}} 2iN_B \left( \frac{\varepsilon - \mu_r}{k_B T_r} \right) \text{Im}(\Sigma_r^R(\varepsilon)), \end{aligned} \quad (9)$$

where  $N_B(x) = \frac{1}{e^x - 1}$  is Bose-Einstein distribution. Then we can calculate bulk magnon current using Heisenberg motion equation.

$$\hbar \frac{d\langle \alpha_i^\dagger \alpha_i \rangle}{dt} = \sum_j -i(h_{i,j}\rho_{j,i} - h_{j,i}\rho_{i,j}) = \sum_j j_{m;i,j}, \quad (10)$$

where  $j_{m;i,j}$  represents the magnon current from site  $i$  to site  $j$ ,  $h_{i,j} = A_0\delta_{i,j} + A_2\delta_{i,j\pm 2}$  is Hamiltonian for  $\alpha$  mode magnons. Eq. (10) indicates that the change of the magnon number at site  $i$  is equal to all magnon currents from site  $i$  to other sites.

According to Ref. [22], The reversal of the FM layer magnetization does not affect the transport of magnon generated

by the spin Hall effect (SHE). However, for magnon current induced by the spin Seebeck effect (SSE), the reversal of the FM layer magnetization leads to a opposite output signal. Therefore we assume that magnons with opposite polarity experience an equivalent spin chemical potential step but an opposite temperature gradient.

The Green's function formalism can also be utilized to calculate the interface magnon current. By using the Landauer-Büttiker formula [44], we find that the magnon current at the interface between AFMI and NMs can be expressed as follows:

$$\begin{aligned} j_{L(R)}^m &= j_{L(R),\alpha}^m + j_{L(R),\beta}^m \\ &= \int \frac{d\varepsilon}{2\pi} \left[ N_B \left( \frac{\varepsilon - \mu_{L(R)}}{k_B T_{L(R)}} \right) - N_B \left( \frac{\varepsilon - \mu_{R(L)}}{k_B T_{R(L)}} \right) \right] T_{b,\alpha}(\varepsilon) \\ &\quad + \int \frac{d\varepsilon}{2\pi} \left[ N_B \left( \frac{\varepsilon - \mu_{L(R)}}{k_B T_{L(R)}} \right) - N_B \left( \frac{\varepsilon - \mu_C}{k_B T_{AFMI}} \right) \right] T_{f,\alpha}(\varepsilon) \\ &\quad + \int \frac{d\varepsilon}{2\pi} \left[ N_B \left( \frac{\varepsilon - \mu_{L(R)}}{k_B T_{R(L)}} \right) - N_B \left( \frac{\varepsilon - \mu_{R(L)}}{k_B T_{L(R)}} \right) \right] T_{b,\beta}(\varepsilon) \\ &\quad + \int \frac{d\varepsilon}{2\pi} \left[ N_B \left( \frac{\varepsilon - \mu_{L(R)}}{k_B T_{AFMI}} \right) - N_B \left( \frac{\varepsilon - \mu_C}{k_B T_{L(R)}} \right) \right] T_{f,\beta}(\varepsilon), \end{aligned} \quad (11)$$

where the transmission function

$$\begin{aligned} T_{b,i}(\varepsilon) &\equiv \text{Tr}[\hbar \Gamma_{L(R),i}(\varepsilon) \mathcal{G}_i^R(\varepsilon) \hbar \Gamma_{R(L),i}(\varepsilon) \mathcal{G}_i^A(\varepsilon)], \\ T_{f,i}(\varepsilon) &\equiv \text{Tr}[\hbar \Gamma_{L(R),i}(\varepsilon) \mathcal{G}_i^R(\varepsilon) \hbar \Gamma_{AFMI,i}(\varepsilon) \mathcal{G}_i^A(\varepsilon)], \end{aligned} \quad (12)$$

where  $i = \alpha$  or  $\beta$ , are two modes of magnons with opposite polarity, the rates  $\Gamma_{L(R),i}(\varepsilon) = -2\text{Im}(\Sigma_{L(R),i}^R(\varepsilon))$ .

The Green's function formalism can be utilized to calculate magnon current driven by temperature gradient or spin chemical potential gradient. In particular, we use temperature difference between left and right NMs to simulate magnon current excited by SEE, and use spin chemical difference between left and right NMs to simulate magnon current excited by SHE.

### III. RESULTS AND DISCUSSIONS

To investigate the spatial distribution and temperature dependence of magnon currents in AFMI excited by the SSE and the SHE, we set the temperature difference  $\Delta T$  and spin chemical potential difference  $\Delta\mu$  between two NMs. In Fig. 3(a), we calculated spatial distribution of magnon currents excited by SSE in AFMI. The parameters used in simulation are set to be  $A_0 = B_0 = 0.5$  eV,  $A_2 = B_2 = -0.25$  eV,  $N = 100$ ,  $h_{\text{ext}} = 0$ ,  $\mu_L = \mu_R = 0$ ,  $\eta^L = \eta^R = 8$ ,  $k_B T_{AFMI} = 0.026$  eV,  $T_L = 1.2 T_{AFMI}$ ,  $T_R = 0.8 T_{AFMI}$ ,  $\mu_{AFMI} = 0$ , and  $\alpha_{AFMI} = 0.001$  [48]. We can see that the magnon currents composed of  $\alpha$  and  $\beta$  modes magnons have different sign but the same absolute value, so the  $\alpha$  and  $\beta$  mode magnon currents cancel with each other, total magnon current  $j_m^{\text{sum}}$  is 0. Then we keep the temperature of left NM  $T_L = 1.2 T_{AFMI}$  fixed, change the temperature of right NM  $T_R$ , and average all the  $\alpha$  mode magnon current at 100 sites, the temperature dependence of averaged  $\alpha$  mode magnon currents  $\bar{j}_m^\alpha$  is shown in Fig. 3(b), we can see that  $\bar{j}_m^\alpha$  shows positive correlation dependence

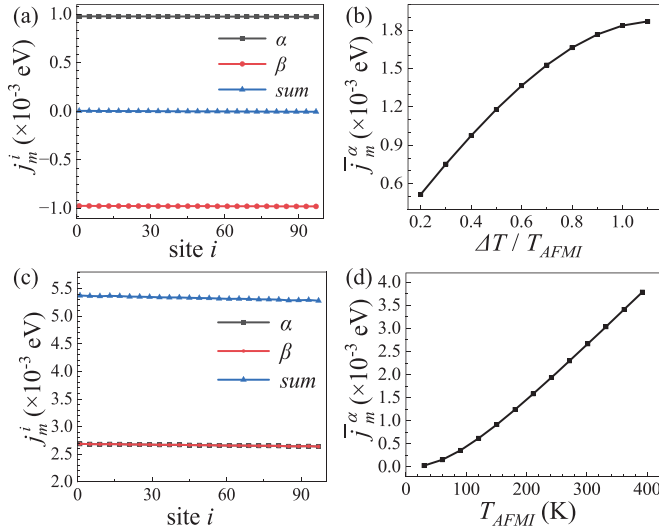


FIG. 3. Spatial distribution and temperature dependence of magnon currents excited by SSE [(a) and (b)] and SHE [(c) and (d)] in AFMI. The spin chemical potential of two normal metals and temperature profile are set to be (a)  $\mu_L = \mu_R = 0$ ,  $k_B T_{AFMI} = 0.026$  eV,  $T_L = 1.2 T_{AFMI}$ ,  $T_R = 0.8 T_{AFMI}$ , and (c)  $\mu_L = 0.1 A_0$ ,  $\mu_R = 0$ ,  $k_B T_{AFMI} = 0.026$  eV,  $T_L = T_R = T_{AFMI}$ .

on temperature difference between left and right NMs  $\Delta T = T_L - T_R$  and the influence of  $\Delta T$  on  $\bar{j}_m^\alpha$  is gradually reduced as  $\Delta T$  increases. Then we calculated spatial distribution of magnon currents excited by SHE in AFMI, see Fig. 3(c). Spin chemical potential  $\mu_L = 0.1 A_0$ ,  $\mu_R = 0$ , temperature  $k_B T_{AFMI} = 0.026$  eV,  $T_L = T_R = T_{AFMI}$ . We can see that for magnon current excited by SHE,  $\alpha$  and  $\beta$  mode magnons contribute equally in the component of sum magnon currents. And then we change the temperature of left NM, AFMI, and right NM at the same time, and calculate the temperature dependence of average  $\alpha$  mode magnon current, as shown in Fig. 3(d). We can see that  $\bar{j}_m^\alpha$  increases as  $T_{AFMI}$  increases. It can be explained by that as  $T_{AFMI}$  increase, the number of  $\alpha$  mode magnon in sublattice  $n_\alpha(\epsilon) = \frac{1}{e^{\beta \epsilon} - 1}$  increases, therefore, the magnons involved in transport increase.

Then we calculate the spatial distribution and temperature dependence of magnon currents in FIMI excited by the SSE and the SHE. In Fig. 4(a), we calculated spatial distribution of magnon currents excited by SSE in FIMI. The parameters used in simulation are set to be  $A_0 = 1.3$  eV,  $B_0 = 0.43$  eV,  $A_2 = -0.6$  eV,  $B_2 = -0.2$  eV,  $N = 100$ ,  $h_{ext} = 0$ ,  $\mu_L = \mu_R = 0$ ,  $\eta^L = \eta^R = 8$ ,  $k_B T_{FIMI} = 0.026$  eV,  $T_L = 1.2 T_{FIMI}$ ,  $T_R = 0.8 T_{FIMI}$ ,  $\mu_{FIMI} = 0$  and  $\alpha_{FIMI} = 0.001$ . We can see that although magnon currents generated by  $\alpha$  and  $\beta$  mode magnons have opposite sign, they do not cancel with each other. Then we keep left NM temperature  $T_L = 1.2 T_{FIMI}$  fixed, change the right NM temperature  $T_R$ , calculate the site average magnon current  $\bar{j}_m^\alpha$ ,  $\bar{j}_m^\beta$ ,  $\bar{j}_m^{sum}$  dependence on the temperature difference, see Fig. 4(b) we can see the absolute value of  $\bar{j}_m^\alpha$ ,  $\bar{j}_m^\beta$ ,  $\bar{j}_m^{sum}$  increase as temperature difference between left and right NMs  $\Delta T$  increases. As for magnon current excited by SHE in FIMI, we set parameters to be spin chemical potential  $\mu_L = 0.1 A_0$ ,  $\mu_R = 0$ ,

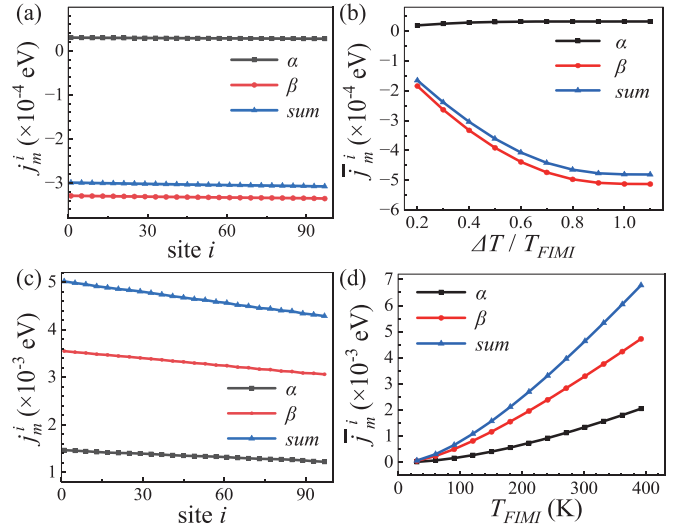


FIG. 4. Spatial distribution and temperature dependence of magnon currents excited by SSE [(a) and (b)] and SHE [(c) and (d)] in FIMI. The spin chemical potential of two normal metals and temperature profile are set to be (a)  $\mu_L = \mu_R = 0$ ,  $k_B T_{FIMI} = 0.026$  eV,  $T_L = 1.2 T_{FIMI}$ ,  $T_R = 0.8 T_{FIMI}$ , and (c)  $\mu_L = 0.1 A_0$ ,  $\mu_R = 0$ ,  $k_B T_{FIMI} = 0.026$  eV,  $T_L = T_R = T_{FIMI}$ .

temperature  $k_B T_{FIMI} = 0.026$  eV,  $T_L = T_R = T_{FIMI}$ , and calculate the space distribution of magnon current. We can see from Fig. 4(c) that in FIMI due to the difference of on-site and next-nearest transition energy between  $\alpha$  and  $\beta$  mode magnons, the magnon currents composed by these two types of magnons are not the same. And then we change the temperature of the whole system at the same time, and calculate the temperature dependence of average magnon current  $\bar{j}_m^\alpha$ ,  $\bar{j}_m^\beta$ ,  $\bar{j}_m^{sum}$ . We can see from Fig. 4(d) that  $\bar{j}_m^\alpha$ ,  $\bar{j}_m^\beta$ ,  $\bar{j}_m^{sum}$  all increase as system temperature increase, which is due to the increase of magnons in two sublattices.

Using the same method above, we can calculate magnon currents in magnon junction, the model includes a magnon junction and two NM leads, as shown in Fig. 5. The boundary conditions are set to be that magnon currents are continuous at interface between FMI1 and AFMI1, between AFMI and FMI2. And the magnon current injected from NM1 to FMI1 is set to be zero, which excluded the influence of spin current injected from NM1 on output magnon current. The boundary conditions are the set of equations relating  $\mu_{FMI1}$ ,  $\mu_{AFMI}$ , and  $\mu_{FMI2}$ . From this system of equations, we can determine the values of  $\mu_{FMI1}$ ,  $\mu_{AFMI}$ , and  $\mu_{FMI2}$ . (Details of calculation are shown in Appendix C).

For parallel magnetization, magnon potentials are  $\mu_{FMI1} = 20$  meV,  $\mu_{AFMI} = 5.3$  meV,  $\mu_{FMI2} = 18$  meV, and the magnon current at the interface of FMI2 and NM2 is  $6.53 \times 10^{-4}$  eV; for antiparallel magnetization state, magnon potentials are  $\mu_{FMI1} = -37$  meV,  $\mu_{AFMI} = 5.2$  meV,  $\mu_{FMI2} = -36.8$  meV, and the magnon current at the interface of FMI2 and NM2 is  $4.79 \times 10^{-7}$  eV. It shows near 100% magnon junction ratio, here magnon junction ratio is  $MJR = (J_{m,\uparrow\uparrow} - J_{m,\uparrow\downarrow}) / (J_{m,\uparrow\uparrow} + J_{m,\uparrow\downarrow})$ , where  $J_{m,\uparrow\uparrow}$  and  $J_{m,\uparrow\downarrow}$  are output magnon current of parallel magnetization and antiparallel magnetization state.



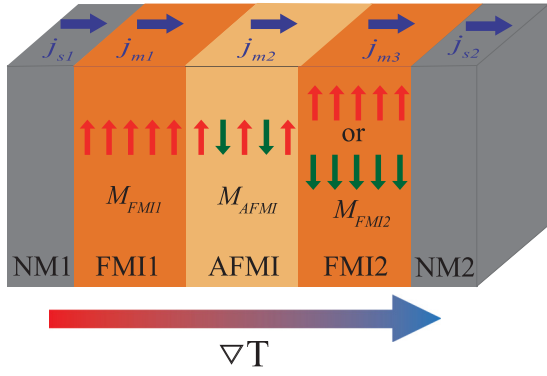


FIG. 5. Schematic diagram of magnon current driven by temperature gradient transporting through a magnon junction.

#### IV. CONCLUSIONS

In conclusion, we propose a Green's function formalism as a comprehensive quantum theory for investigating magnon transport in AFMIs or FIMIs, specifically tailored for two-sublattice magnetic systems. We studied the spatial distribution and temperature dependence of the magnon current induced by temperature or spin chemical potential step in FIMIs or AFMIs. Our results reveal that the magnon currents in both sublattices exhibit a positive correlation with temperature. Interestingly, in AFMI, the magnon currents generated by temperature step in the two sublattices cancel each other out. Furthermore, we numerically simulate the magnon junction effect using the Green's function formalism, which yields a near 100% magnon junction ratio. Our work demonstrates the potential of employing comprehensive quantum theory to unravel the intricacies of magnon transport in specific magnonic devices.

#### ACKNOWLEDGMENTS

This work is financial supported by the National Key Research and Development Program of China (MOST) (Grant No. 2022YFA1402800), the National Natural Science Foundation of China (NSFC) (Grants No. 51831012 and No. 12134017), and partially supported by the Strategic Priority Research Program (B) (Grant No. XDB33000000).

#### APPENDIX A: DERIVATION OF EQ. (2)

The Hamiltonian of FIMI or AFMI, considering the nearest neighbor and next-nearest neighbor Heisenberg exchange interactions, can be expressed as follows:

$$\begin{aligned} \hat{H} = & -J_{AB} \sum_{\langle i,m \rangle} \hat{S}_i \cdot \hat{S}_m - J_A \sum_{\langle\langle i,j \rangle\rangle} \hat{S}_i \cdot \hat{S}_j \\ & - J_B \sum_{\langle\langle m,n \rangle\rangle} \hat{S}_m \cdot \hat{S}_n - h_{\text{ext}} \left( \sum_i \mu_A \hat{S}_i^z + \sum_m \mu_B \hat{S}_m^z \right), \end{aligned} \quad (\text{A1})$$

where  $\langle \rangle$  denotes summing over nearest sites,  $\langle\langle \rangle\rangle$  denotes summing over next-nearest sites.  $J_{AB}$  and  $J_{A(B)}$  represent the nearest and next-nearest Heisenberg exchange interactions strength, respectively.  $S_{i(m)}$  is the spin in A(B) sublattice,

$\mu_{A(B)}$  is the magnetic moment in A(B) sublattice.  $h_{\text{ext}}$  is applied magnetic field along the z direction. Using Holstein-Primakoff (HP) transformation, we can get

$$\begin{aligned} \hat{S}_i^+ &= \sqrt{2S_A - \hat{a}_i^\dagger \hat{a}_i} \hat{a}_i, & \hat{S}_i^- &= \hat{a}_i^\dagger \sqrt{2S_A - \hat{a}_i^\dagger \hat{a}_i}, \\ \hat{S}_i^z &= S_A - \hat{a}_i^\dagger \hat{a}_i, & \hat{S}_m^+ &= \hat{b}_m^\dagger \sqrt{2S_B - \hat{b}_m^\dagger \hat{b}_m}, \\ \hat{S}_m^- &= \sqrt{2S_B - \hat{b}_m^\dagger \hat{b}_m} \hat{b}_m, & \hat{S}_m^z &= \hat{b}_m^\dagger \hat{b}_m - S_B, \end{aligned} \quad (\text{A2})$$

where  $\hat{a}_i$  ( $\hat{b}_m$ ),  $\hat{a}_i^\dagger$  ( $\hat{b}_m^\dagger$ ) are magnon annihilation and creation operators in A(B) sublattice, respectively. By substituting Eq. (A2) into Eq. (A1), we can reform the Hamiltonian of FIMI or AFMI using magnon annihilation and creation operators and get

$$\begin{aligned} \hat{H} = & -J_{AB} \sqrt{S_A S_B} \sum_{\langle i,m \rangle} (\hat{a}_i \hat{b}_m + \hat{a}_i^\dagger \hat{b}_m^\dagger) - J_A \sum_{\langle\langle i,j \rangle\rangle} S_A (\hat{a}_i \hat{a}_j^\dagger + \hat{a}_i^\dagger \hat{a}_j) \\ & - J_B \sum_{\langle\langle m,n \rangle\rangle} S_B (\hat{b}_m^\dagger \hat{b}_n + \hat{b}_m \hat{b}_n^\dagger) \\ & - \sum_i (J_{AB} S_B N_n - 2J_A S_A N_{nm} - h_{\text{ext}} \mu_A) \hat{a}_i^\dagger \hat{a}_i \\ & - \sum_m (J_{AB} S_A N_n - 2J_B S_B N_{nm} + h_{\text{ext}} \mu_B) \hat{b}_m^\dagger \hat{b}_m + \text{const}, \end{aligned} \quad (\text{A3})$$

where  $N_n$ ,  $N_{nm}$  are the numbers of nearest and the next-nearest sites, respectively. In the case of a one-dimensional atomic chain model,  $N_n = N_{nm} = 2$ . Using Fourier transformation for magnon annihilation and creation operators

$$\begin{aligned} \hat{a}_i &= \frac{1}{\sqrt{N}} \sum_k e^{ik \cdot \mathbf{R}_i} \hat{a}_k, & \hat{a}_i^\dagger &= \frac{1}{\sqrt{N}} \sum_k e^{-ik \cdot \mathbf{R}_i} \hat{a}_k^\dagger, \\ \hat{b}_m &= \frac{1}{\sqrt{N}} \sum_k e^{-ik \cdot \mathbf{R}_m} \hat{b}_k, & \hat{b}_m^\dagger &= \frac{1}{\sqrt{N}} \sum_k e^{ik \cdot \mathbf{R}_m} \hat{b}_k^\dagger, \end{aligned} \quad (\text{A4})$$

we can get

$$\begin{aligned} \hat{H} = & \sum_k [-J_{AB} \sqrt{S_A S_B} \gamma_{k,n} (\hat{a}_k \hat{b}_k + \hat{a}_k^\dagger \hat{b}_k^\dagger)] \\ & + \sum_k (-2J_A S_A \gamma_{k,nn} \hat{a}_k^\dagger \hat{a}_k - 2J_B S_B \gamma_{k,nn} \hat{b}_k^\dagger \hat{b}_k) \\ & + \sum_k (-J_{AB} S_B N_n + 2J_A S_A N_{nm} + h_{\text{ext}} \mu_A) \hat{a}_k^\dagger \hat{a}_k \\ & + \sum_k (-J_{AB} S_A N_n + 2J_B S_B N_{nm} - h_{\text{ext}} \mu_B) \hat{b}_k^\dagger \hat{b}_k + \text{const} \\ = & \sum_k (-2J_A S_A \gamma_{k,nn} - J_{AB} S_B N_n + 2J_A S_A N_{nm} + h_{\text{ext}} \mu_A) \hat{a}_k^\dagger \hat{a}_k \\ & + \sum_k (-2J_B S_B \gamma_{k,nn} - J_{AB} S_A N_n + 2J_B S_B N_{nm} - h_{\text{ext}} \mu_B) \hat{b}_k^\dagger \hat{b}_k \\ & + \sum_k [-J_{AB} \sqrt{S_A S_B} \gamma_{k,n} (\hat{a}_k \hat{b}_k + \hat{a}_k^\dagger \hat{b}_k^\dagger)] + \text{const} \\ \equiv & \sum_k [A_k \hat{a}_k^\dagger \hat{a}_k + B_k \hat{b}_k^\dagger \hat{b}_k + C_k (\hat{a}_k \hat{b}_k + \hat{a}_k^\dagger \hat{b}_k^\dagger)] + \text{const}, \end{aligned} \quad (\text{A5})$$

where  $\gamma_{k,n} = \sum_{\delta_n} e^{-ik \cdot \delta_n}$ ,  $\gamma_{k,nn} = \sum_{\delta_{nn}} e^{-ik \cdot \delta_{nn}}$ . For a one-dimensional atomic chain model,  $\gamma_{k,n} = 2 \cos(ka)$ ,  $\gamma_{k,nn} = 2 \cos(2ka)$ , where  $a$  is the distance between nearest sites,  $A_k \equiv -2J_A S_A \gamma_{k,nn} - J_{AB} S_B N_n + 2J_A S_A N_{nn} + h_{\text{ext}} \mu_A$ ,  $B_k \equiv -2J_B S_B \gamma_{k,nn} - J_{AB} S_A N_n + 2J_B S_B N_{nn} - h_{\text{ext}} \mu_B$ , and  $C_k \equiv -J_{AB} \sqrt{S_A S_B} \gamma_{k,n}$ .

Using Bogoliubov transformation,

$$\begin{aligned} \hat{a}_k &= u_k \hat{\alpha}_k + v_k \hat{\beta}_k^\dagger, & \hat{a}_k^\dagger &= u_k \hat{\alpha}_k^\dagger + v_k \hat{\beta}_k, \\ \hat{b}_k &= u_k \hat{\beta}_k + v_k \hat{\alpha}_k^\dagger, & \hat{b}_k^\dagger &= u_k \hat{\beta}_k^\dagger + v_k \hat{\alpha}_k, \\ \hat{\alpha}_k &= u_k \hat{a}_k - v_k \hat{b}_k^\dagger, & \hat{\alpha}_k^\dagger &= u_k \hat{a}_k^\dagger - v_k \hat{b}_k, \\ \hat{\beta}_k &= u_k \hat{b}_k - v_k \hat{a}_k^\dagger, & \hat{\beta}_k^\dagger &= u_k \hat{b}_k^\dagger - v_k \hat{a}_k. \end{aligned} \quad (\text{A6})$$

With commutation relationship  $[\hat{\alpha}_k, \hat{\alpha}_{k'}^\dagger] = [\hat{\beta}_k, \hat{\beta}_{k'}^\dagger] = \delta_{k,k'}$ ,  $[\hat{\alpha}_k, \hat{\beta}_{k'}^\dagger] = [\hat{\alpha}_k^\dagger, \hat{\beta}_{k'}] = [\hat{\alpha}_k^\dagger, \hat{\beta}_{k'}^\dagger] = 0$  and relationship  $u_k^2 - v_k^2 = 1$ , we can get

$$\begin{aligned} \hat{H} &= \sum_k [(A_k u_k^2 + B_k v_k^2 + 2C_k u_k v_k) \hat{\alpha}_k^\dagger \hat{\alpha}_k \\ &+ (A_k u_k v_k + B_k u_k v_k + C_k (u_k^2 + v_k^2)) \hat{\alpha}_k^\dagger \hat{\beta}_k^\dagger \\ &+ (A_k u_k v_k + B_k u_k v_k + C_k (u_k^2 + v_k^2)) \hat{\alpha}_k \hat{\beta}_k \\ &+ (A_k v_k^2 + B_k u_k^2 + 2C_k u_k v_k) \hat{\beta}_k^\dagger \hat{\beta}_k] + \text{const}. \end{aligned} \quad (\text{A7})$$

Take

$$\begin{aligned} u_k &= -\sqrt{\frac{1}{2} + \frac{A_k + B_k}{2\sqrt{(A_k + B_k)^2 - 4C_k^2}}}, \\ v_k &= \sqrt{-\frac{1}{2} + \frac{A_k + B_k}{2\sqrt{(A_k + B_k)^2 - 4C_k^2}}}, \end{aligned} \quad (\text{A8})$$

$$\begin{aligned} w_k^\alpha &= \frac{-4(J_A S_A - J_B S_B) \cos(2ka) - J_{AB}(S_B - S_A)N_n + 2(J_A S_A - J_B S_B)N_{nn} + h_{\text{ext}}(\mu_A - \mu_B)}{2} \\ &+ \frac{\sqrt{[-4(J_A S_A + J_B S_B) \cos(2ka) - J_{AB}(S_B + S_A)N_n + 2(J_A S_A + J_B S_B)N_{nn} + h_{\text{ext}}(\mu_A + \mu_B)]^2 - 8J_A S_A S_B (\cos(2ka) + 1)}}{2}. \end{aligned} \quad (\text{B4})$$

And we can see from Eq. (B4) that  $w^\alpha(\pi - x) = w^\alpha(x)$ , since  $\cos(i(\pi - x)) = (-1)^i \cos(ix)$ , we can get that

$$\begin{aligned} A_i &= \frac{1}{2\pi} \int_{-\pi}^{\pi} w^\alpha(\pi - t) \cos(i(\pi - t)) dt \\ &= (-1)^i \frac{1}{2\pi} \int_{-\pi}^{\pi} w^\alpha(t) \cos(it) dt \\ &= (-1)^i \frac{1}{2\pi} \left[ \int_{-\pi}^0 w^\alpha(t) \cos(it) dt + \int_0^{\pi} w^\alpha(t) \cos(it) dt \right]. \end{aligned} \quad (\text{B5})$$

And  $\int_{-\pi}^0 w^\alpha(t) \cos(it) dt = \int_{\pi}^{2\pi} w^\alpha(t) \cos(it) dt$ , so we can get

$$A_i = (-1)^i \frac{1}{2\pi} \int_0^{2\pi} w^\alpha(t) \cos(it) dt = (-1)^i A_i. \quad (\text{B6})$$

$$\begin{aligned} \hat{H} &= \sum_k \left[ \frac{A_k - B_k}{2} + \frac{\sqrt{(A_k + B_k)^2 - 4C_k^2}}{2} \right] \hat{\alpha}_k^\dagger \hat{\alpha}_k \\ &\equiv + \left[ \frac{-A_k + B_k}{2} + \frac{\sqrt{(A_k + B_k)^2 - 4C_k^2}}{2} \right] \hat{\beta}_k^\dagger \hat{\beta}_k + \text{const} \\ &\equiv \sum_k w_k^\alpha \hat{\alpha}_k^\dagger \hat{\alpha}_k + w_k^\beta \hat{\beta}_k^\dagger \hat{\beta}_k + \text{const}. \end{aligned} \quad (\text{A9})$$

## APPENDIX B: DERIVATION OF $A_{2i+1} = B_{2i+1} = 0$

Let's take  $\alpha$  mode magnon as an example, we will prove  $A_{2i+1} = 0$ . Similarly, we can also prove  $B_{2i+1} = 0$  by using the same method. The expression for  $w_k^\alpha$  is

$$w_k^\alpha = \frac{A_k - B_k}{2} + \frac{\sqrt{(A_k + B_k)^2 - 4C_k^2}}{2}, \quad (\text{B1})$$

where

$$\begin{aligned} A_k &\equiv -2J_A S_A \gamma_{k,nn} - J_{AB} S_B N_n + 2J_A S_A N_{nn} + h_{\text{ext}} \mu_A, \\ B_k &\equiv -2J_B S_B \gamma_{k,nn} - J_{AB} S_A N_n + 2J_B S_B N_{nn} - h_{\text{ext}} \mu_B, \\ C_k &\equiv -J_{AB} \sqrt{S_A S_B} \gamma_{k,n}. \end{aligned} \quad (\text{B2})$$

$J_{AB} < 0$  and  $J_{A(B)} > 0$  represent the nearest and next-nearest exchange interactions in the A(B) sublattices,  $S_{A(B)}$  is the spin in A(B) sublattice,  $\mu_{A(B)}$  is the magnetic moment in A(B) sublattice.  $h_{\text{ext}}$  is applied magnetic field,  $N_n, N_{nn}$  are the numbers of nearest and the next-nearest sites. And in the case of one-dimensional atomic chain model

$$\gamma_{k,n} = 2 \cos(ka) \text{ and } \gamma_{k,nn} = 2 \cos(2ka). \quad (\text{B3})$$

Substitute Eq. (B2) and (B3) in (B1), we can get

So we can get  $A_{2i+1} = 0$ . Using the same method, we can prove  $B_{2i+1} = 0$ .

## APPENDIX C: CALCULATION OF MAGNON JUNCTION EFFECT

The Hamiltonian of the magnon junction is composed of five items

$$\hat{H} = \hat{H}_{\text{FMI1}} + \hat{H}_{\text{AFMI}} + \hat{H}_{\text{FMI2}} + \hat{H}_{\text{FMI1,AFMI}} + \hat{H}_{\text{FMI2,AFMI}}. \quad (\text{C1})$$

where  $\hat{H}_{\text{FMI1}}, \hat{H}_{\text{AFMI}}, \hat{H}_{\text{FMI2}}$  are Hamiltonian of FMI1, AFMI and FMI2, respectively, and  $\hat{H}_{\text{FMI1,AFMI}}, \hat{H}_{\text{FMI2,AFMI}}$  are coupling between FMI1 and AFMI, FMI2 and AFMI, re-

spectively. Only on-site and next-nearest transition energy are considered. For parallel state,

$$\hat{H}_{\text{FMI1}(2)} = \sum_{i,j} [(A_0^{\text{FMI1}(2)} \delta_{i,j} + A_2^{\text{FMI1}(2)} \delta_{i,j\pm 2})] \hat{\alpha}_i^\dagger \hat{\alpha}_j, \quad (\text{C2})$$

$$\begin{aligned} \hat{H}_{\text{AFMI}} = & \sum_{i,j} [(A_0^{\text{AFMI}} \delta_{i,j} + A_2^{\text{AFMI}} \delta_{i,j\pm 2})] \hat{\alpha}_i^\dagger \hat{\alpha}_j \\ & + (B_0^{\text{AFMI}} \delta_{i,j} + B_2^{\text{AFMI}} \delta_{i,j\pm 2}) \hat{\beta}_i^\dagger \hat{\beta}_j, \end{aligned} \quad (\text{C3})$$

$$\begin{aligned} \hat{H}_{\text{FMI1}(2),\text{AFMI}} = & J_{\text{FMI1}(2),\text{AFMI}} (\hat{\alpha}_{\text{end}(1),\text{FMI1}(2)}^\dagger \\ & \hat{\alpha}_{1(\text{end}),\text{AFMI}} + \hat{\alpha}_{\text{end}(1),\text{FMI1}(2)}^\dagger \\ & \hat{\beta}_{1(\text{end}),\text{AFMI}}) + \text{H.c.}, \end{aligned} \quad (\text{C4})$$

and for antiparallel state, all the  $\hat{\alpha}$  ( $\hat{\alpha}^\dagger$ ) in Hamiltonian of  $\hat{H}_{\text{FMI2}}$  and  $\hat{\alpha}_{\text{FMI2}}$  ( $\hat{\alpha}_{\text{FMI2}}^\dagger$ ) in Hamiltonian of  $\hat{H}_{\text{FMI2},\text{AFMI}}$  are replaced by  $\hat{\beta}$  ( $\hat{\beta}^\dagger$ ) and  $\hat{\beta}_{\text{FMI2}}$  ( $\hat{\beta}_{\text{FMI2}}^\dagger$ ).

We can use Eqs. (11), (12), and (C1)–(C4) to calculate magnon currents in three parts of magnon junction. The boundary conditions are set to be that magnon currents are continuous at interface between FMI1 and AFMI1, between AFMI and FMI2. And the magnon current injected from NM1 to FMI1 is set to be zero, which

excluded the influence of spin current injected from NM1 on output magnon current. The simulation parameters are set to be on-site energy  $A_0^{\text{FMI1}} = A_0^{\text{FMI2}} = A_0^{\text{AFMI}} = B_0^{\text{AFMI}} = 0.5 \text{ eV}$ , nearest transition energy  $A_1^{\text{FMI1}} = A_1^{\text{FMI2}} = -0.5 \text{ eV}$ ,  $A_1^{\text{AFMI}} = B_1^{\text{AFMI}} = -0.25 \text{ eV}$ , coupling energy of two types of magnons  $J_{\text{FMI1},\text{AFMI}} = J_{\text{FMI2},\text{AFMI}} = 1 \text{ eV}$ , spin chemical potential of two NMs layer  $\mu_{\text{NM1}} = \mu_{\text{NM2}} = 0$ , temperature  $k_B T_{\text{NM1}} = 0.026 \text{ eV}$ ,  $T_{\text{FMI1}} = 0.9 T_{\text{NM1}}$ ,  $T_{\text{AFMI}} = 0.8 T_{\text{NM1}}$ ,  $T_{\text{FMI2}} = 0.7 T_{\text{NM1}}$ ,  $T_{\text{NM2}} = 0.6 T_{\text{NM1}}$ , total site number  $N_{\text{FMI1}} = N_{\text{AFMI}} = N_{\text{FMI2}} = 20$ , coupling with two NMs layers  $\eta^{L(R)} = 8$  and Gilbert damping constant  $\alpha_{\text{FMI1}} = \alpha_{\text{FMI2}} = 0.01$ ,  $\alpha_{\text{AFMI}} = 0.001$ .

Boundary condition is a nonlinear system of first order equations, and we can get a rough solution of  $\mu_{\text{FMI1}}$ ,  $\mu_{\text{AFMI}}$ ,  $\mu_{\text{FMI2}}$ . Here we use one-dimensional atomic chain model and assume that the spin chemical potential affect the transport of magnon in AFMI or FMI1 through change the on-site energy of magnons. Different part's retarded self-energy has the following formalism. For FMI1, the left, right and center retarded self-energies are

$$\Sigma_{L,\text{FMI1},j}^R(\varepsilon) = -\frac{i\eta_L(\varepsilon - \mu_{\text{NM1}})}{\hbar} \delta_{i,1} \delta_{j,1}, \quad (\text{C5})$$

$$\Sigma_{R,\text{FMI1},j}^R(\varepsilon) = 2 \frac{J_{\text{FMI1},\text{AFMI}}^2}{(A_2^{\text{AFMI}})^2} \left[ \frac{(\varepsilon - \mu_{\text{AFMI}})}{2} \pm \sqrt{\frac{(\varepsilon - \mu_{\text{AFMI}})^2}{4} - (A_2^{\text{AFMI}})^2} \right] / \hbar \delta_{i,N_{\text{FMI1}}} \delta_{j,N_{\text{FMI1}}}. \quad (\text{C6})$$

The choice of solution is determined by the requirement that  $\text{Im} \Sigma_{R,\text{FMI1},j}^R(\varepsilon) < 0$ :

$$\Sigma_{C,\text{FMI1},j}^R(\varepsilon) = -\frac{i\alpha_{\text{FMI1}}(\varepsilon - \mu_{\text{FMI1}})}{\hbar} \delta_{i,j}. \quad (\text{C7})$$

For AFMI, the left, right, and center retarded self-energies are

$$\Sigma_{L,\text{AFMI},j}^R(\varepsilon) = \frac{J_{\text{FMI1},\text{AFMI}}^2}{(A_2^{\text{FMI1}})^2} \left[ \frac{(\varepsilon - \mu_{\text{FMI1}})}{2} \pm \sqrt{\frac{(\varepsilon - \mu_{\text{FMI1}})^2}{4} - (A_2^{\text{FMI1}})^2} \right] / \hbar \delta_{i,1} \delta_{j,1}, \quad (\text{C8})$$

$$\Sigma_{R,\text{AFMI},j}^R(\varepsilon) = \frac{J_{\text{FMI2},\text{AFMI}}^2}{(A_2^{\text{FMI2}})^2} \left[ \frac{(\varepsilon - \mu_{\text{FMI2}})}{2} \pm \sqrt{\frac{(\varepsilon - \mu_{\text{FMI2}})^2}{4} - (A_2^{\text{FMI2}})^2} \right] / \hbar \delta_{i,N_{\text{AFMI}}} \delta_{j,N_{\text{AFMI}}}. \quad (\text{C9})$$

The choice of solution is determined by the requirement that  $\text{Im} \Sigma_{L,\text{AFMI},j}^R(\varepsilon)$  and  $\text{Im} \Sigma_{R,\text{AFMI},j}^R(\varepsilon) < 0$ .

$$\Sigma_{C,\text{AFMI},j}^R(\varepsilon) = -\frac{i\alpha_{\text{AFMI}}(\varepsilon - \mu_{\text{AFMI}})}{\hbar} \delta_{i,j} \quad (\text{C10})$$

For FMI2, the left, right, and center retarded self-energies are

$$\Sigma_{L,\text{FMI2},j}^R(\varepsilon) = 2 \frac{J_{\text{FMI2},\text{AFMI}}^2}{(A_2^{\text{AFMI}})^2} \left[ \frac{(\varepsilon - \mu_{\text{AFMI}})}{2} \pm \sqrt{\frac{(\varepsilon - \mu_{\text{AFMI}})^2}{4} - (A_2^{\text{AFMI}})^2} \right] / \hbar \delta_{i,1} \delta_{j,1}. \quad (\text{C11})$$

The choice of solution is determined by the requirement that  $\text{Im} \Sigma_{L,\text{FMI2},j}^R(\varepsilon) < 0$ .

$$\Sigma_{R,\text{FMI2},j}^R(\varepsilon) = -\frac{i\eta_R(\varepsilon - \mu_{\text{NM2}})}{\hbar} \delta_{i,N_{\text{FMI2}}} \delta_{j,N_{\text{FMI2}}}, \quad (\text{C12})$$

$$\Sigma_{C,\text{FMI2},j}^R(\varepsilon) = -\frac{i\alpha_{\text{FMI2}}(\varepsilon - \mu_{\text{FMI2}})}{\hbar} \delta_{i,j}. \quad (\text{C13})$$

- [1] A. V. Chumak, V. I. Vasyuchka, A. A. Serga, and B. Hillebrands, Magnon spintronics, *Nat. Phys.* **11**, 453 (2015).
- [2] H. Y. Yuan, Y. Cao, A. Kamra, R. A. Duine, and P. Yan, Quantum magnonics: When magnon spintronics meets quantum information science, *Phys. Rep.* **965**, 1 (2022).
- [3] F. Bloch, Zur theorie des ferromagnetismus, *Z. Phys.* **61**, 206 (1930).
- [4] J. Xiao, G. E. W. Bauer, K.-c. Uchida, E. Saitoh, and S. Maekawa, Theory of magnon-driven spin seebeck effect, *Phys. Rev. B* **81**, 214418 (2010).
- [5] J. D. Adam, Analog signal processing with microwave magnetics, *Proc. IEEE* **76**, 159 (1988).
- [6] V. Cherepanov, I. Kolokolov, and V. L'vov, The saga of yig: Spectra, thermodynamics, interaction and relaxation of magnons in a complex magnet, *Phys. Rep.* **229**, 81 (1993).
- [7] J. M. Owens, J. H. Collins, and R. L. Carter, System applications of magnetostatic wave devices, *Circuits Syst. Signal Process* **4**, 317 (1985).
- [8] T. Balashov, P. Buczek, L. Sandratskii, A. Ernst, and W. Wulfhekel, Magnon dispersion in thin magnetic films, *J. Phys.: Condens. Matter* **26**, 394007 (2014).
- [9] T.-H. Chuang, Kh. Zakeri, A. Ernst, Y. Zhang, H. J. Qin, Y. Meng, Y.-J. Chen, and J. Kirschner, Magnetic properties and magnon excitations in Fe(001) films grown on Ir(001), *Phys. Rev. B* **89**, 174404 (2014).
- [10] T. Schneider, A. A. Serga, T. Neumann, B. Hillebrands, and M. P. Kostylev, Phase reciprocity of spin-wave excitation by a microstrip antenna, *Phys. Rev. B* **77**, 214411 (2008).
- [11] M. Jamali, J. H. Kwon, S. M. Seo, K. J. Lee, and H. Yang, Spin wave nonreciprocity for logic device applications, *Sci. Rep.* **3**, 3160 (2013).
- [12] V. E. Demidov, M. P. Kostylev, K. Rott, P. Krzysteczko, G. Reiss, and S. O. Demokritov, Excitation of microwaveguide modes by a stripe antenna, *Appl. Phys. Lett.* **95**, 112509 (2009).
- [13] J.-i. Ohe, H. Adachi, S. Takahashi, and S. Maekawa, Numerical study on the spin seebeck effect, *Phys. Rev. B* **83**, 115118 (2011).
- [14] G. E. W. Bauer, E. Saitoh, and B. J. van Wees, Spin caloritronics, *Nat. Mater.* **11**, 391 (2012).
- [15] H. Yu, S. D. Brechet, and J.-P. Ansermet, Spin caloritronics, origin and outlook, *Phys. Lett. A* **381**, 825 (2017).
- [16] S. M. Rezende, R. L. Rodríguez-Suárez, R. O. Cunha, A. R. Rodrigues, F. L. A. Machado, G. A. Fonseca Guerra, J. C. Lopez Ortiz, and A. Azevedo, Magnon spin-current theory for the longitudinal spin-Seebeck effect, *Phys. Rev. B* **89**, 014416 (2014).
- [17] J. Sinova, S. O. Valenzuela, J. Wunderlich, C. H. Back, and T. Jungwirth, Spin hall effects, *Rev. Mod. Phys.* **87**, 1213 (2015).
- [18] S. O. Demokritov, B. Hillebrands, and A. N. Slavin, Brillouin light scattering studies of confined spin waves: linear and non-linear confinement, *Phys. Rep.* **348**, 441 (2001).
- [19] L. K. Werake, B. A. Ruzicka, and H. Zhao, Observation of Intrinsic Inverse Spin Hall Effect, *Phys. Rev. Lett.* **106**, 107205 (2011).
- [20] E. Saitoh, M. Ueda, H. Miyajima, and G. Tatara, Conversion of spin current into charge current at room temperature: Inverse spin-hall effect, *Appl. Phys. Lett.* **88**, 182509 (2006).
- [21] S. S.-L. Zhang and S. Zhang, Magnon Mediated Electric Current Drag Across a Ferromagnetic Insulator Layer, *Phys. Rev. Lett.* **109**, 096603 (2012).
- [22] H. Wu, C. H. Wan, X. Zhang, Z. H. Yuan, Q. T. Zhang, J. Y. Qin, H. X. Wei, X. F. Han, and S. Zhang, Observation of magnon-mediated electric current drag at room temperature, *Phys. Rev. B* **93**, 060403 (2016).
- [23] H. Wu, L. Huang, C. Fang, B. S. Yang, C. H. Wan, G. Q. Yu, J. F. Feng, H. X. Wei, and X. F. Han, Magnon Valve Effect between Two Magnetic Insulators, *Phys. Rev. Lett.* **120**, 097205 (2018).
- [24] L. J. Cornelissen, J. Liu, B. J. van Wees, and R. A. Duine, Spin-Current-Controlled Modulation of the Magnon Spin Conductance in a Three-Terminal Magnon Transistor, *Phys. Rev. Lett.* **120**, 097702 (2018).
- [25] J. Cramer, F. Fuhrmann, U. Ritzmann, V. Gall, T. Niizeki, R. Ramos, Z. Qiu, D. Hou, T. Kikkawa, J. Sinova, U. Nowak, E. Saitoh, and M. Klui, Magnon detection using a ferroic collinear multilayer spin valve, *Nat. Commun.* **9**, 1089 (2018).
- [26] J. Zheng, A. Rückriegel, S. A. Bender, and R. A. Duine, Ellipticity and dissipation effects in magnon spin valves, *Phys. Rev. B* **101**, 094402 (2020).
- [27] C. Y. Guo, C. H. Wan, X. Wang, C. Fang, P. Tang, W. J. Kong, M. K. Zhao, L. N. Jiang, B. S. Tao, G. Q. Yu, and X. F. Han, Magnon valves based on YIG/NiO/YIG all-insulating magnon junctions, *Phys. Rev. B* **98**, 134426 (2018).
- [28] U. Ritzmann, D. Hinzke, and U. Nowak, Propagation of thermally induced magnonic spin currents, *Phys. Rev. B* **89**, 024409 (2014).
- [29] U. Ritzmann, D. Hinzke, and U. Nowak, Thermally induced magnon accumulation in two-sublattice magnets, *Phys. Rev. B* **95**, 054411 (2017).
- [30] T. L. Gilbert, Classics in magnetics a phenomenological theory of damping in ferromagnetic materials, *IEEE Trans. Magn.* **40**, 3443 (2004).
- [31] P. Yan, X. S. Wang, and X. R. Wang, All-Magnonic Spin-Transfer Torque and Domain Wall Propagation, *Phys. Rev. Lett.* **107**, 177207 (2011).
- [32] W. Wang, M. Albert, M. Beg, M.-A. Bisotti, D. Chernyshenko, D. Cortés-Ortuño, I. Hawke, and H. Fangohr, Magnon-Driven Domain-Wall Motion with the Dzyaloshinskii-Moriya Interaction, *Phys. Rev. Lett.* **114**, 087203 (2015).
- [33] J. Lan, W. Yu, R. Wu, and J. Xiao, Spin-Wave Diode, *Phys. Rev. X* **5**, 041049 (2015).
- [34] C. Jia, D. Ma, A. F. Schffer, and J. Berakdar, Twisted magnon beams carrying orbital angular momentum, *Nat. Commun.* **10**, 2077 (2019).
- [35] W. Yu, J. Lan, R. Wu, and J. Xiao, Magnetic snell's law and spin-wave fiber with dzyaloshinskii-moriya interaction, *Phys. Rev. B* **94**, 140410(R) (2016).
- [36] Y. W. Xing, Z. R. Yan, and X. F. Han, Magnon valve effect and resonant transmission in a one-dimensional magnonic crystal, *Phys. Rev. B* **103**, 054425 (2021).
- [37] Z. Wang, Y. Cao, and P. Yan, Goos-Hänchen effect of spin waves at heterochiral interfaces, *Phys. Rev. B* **100**, 064421 (2019).
- [38] S.-J. Lee, J.-H. Moon, H.-W. Lee, and K.-J. Lee, Spin-wave propagation in the presence of inhomogeneous dzyaloshinskii-moriya interactions, *Phys. Rev. B* **96**, 184433 (2017).
- [39] A. Manchon and S. Zhang, Theory of nonequilibrium intrinsic spin torque in a single nanomagnet, *Phys. Rev. B* **78**, 212405 (2008).
- [40] L. J. Cornelissen, K. J. H. Peters, G. E. W. Bauer, R. A. Duine, and B. J. van Wees, Magnon spin transport driven by



- the magnon chemical potential in a magnetic insulator, [Phys. Rev. B \*\*94\*\*, 014412 \(2016\)](#).
- [41] T. Liu, W. Wang, and J. Zhang, Collective induced antidiffusion effect and general magnon boltzmann transport theory, [Phys. Rev. B \*\*99\*\*, 214407 \(2019\)](#).
- [42] J. Sinova, D. Culcer, Q. Niu, N. A. Sinitsyn, T. Jungwirth, and A. H. MacDonald, Universal Intrinsic Spin Hall Effect, [Phys. Rev. Lett. \*\*92\*\*, 126603 \(2004\)](#).
- [43] W. P. Sterk, H. Y. Yuan, A. Rückriegel, B. Z. Rameshti, and R. A. Duine, Green's function formalism for nonlocal elliptical magnon transport, [Phys. Rev. B \*\*104\*\*, 174404 \(2021\)](#).
- [44] J. Zheng, S. Bender, J. Armaitis, R. E. Troncoso, and R. A. Duine, Green's function formalism for spin transport in metal-insulator-metal heterostructures, [Phys. Rev. B \*\*96\*\*, 174422 \(2017\)](#).
- [45] D. Ködderitzsch, W. Hergert, W. M. Temmerman, Z. Szotek, A. Ernst, and H. Winter, Exchange interactions in NiO and at the NiO(100) surface, [Phys. Rev. B \*\*66\*\*, 064434 \(2002\)](#).
- [46] W.-B. Zhang, Y.-L. Hu, K.-L. Han, and B.-Y. Tang, Pressure dependence of exchange interactions in NiO, [Phys. Rev. B \*\*74\*\*, 054421 \(2006\)](#).
- [47] Y. Tserkovnyak, A. Brataas, and G. E. W. Bauer, Enhanced Gilbert Damping in Thin Ferromagnetic Films, [Phys. Rev. Lett. \*\*88\*\*, 117601 \(2002\)](#).
- [48] T. Moriyama, K. Hayashi, K. Yamada, M. Shima, Y. Ohya, and T. Ono, Intrinsic and extrinsic antiferromagnetic damping in NiO, [Phys. Rev. Mater. \*\*3\*\*, 051402\(R\) \(2019\)](#).